GEOPHYSICS, VOL. 79, NO. 5 (SEPTEMBER-OCTOBER 2014); P. WB51–WB61, 8 FIGS., 2 TABLES.
10.1190/GEO2013-0432.1

Kirchhoff modeling for attenuative anisotropic media using Gaussian beams

Bharath Shekar[1] and Ilya Tsvankin[2]

ABSTRACT

Seismic wave propagation in attenuative media can be efficiently modeled with ray-based methods. We present a methodology to generate reflection data from attenuative anisotropic media using the Kirchhoff scattering integral and summation of Gaussian beams. The Green's functions are computed in the reference elastic model by Gaussian-beam summation, and the influence of attenuation is incorporated as a perturbation along the central ray. The reflected P-wave is obtained by substituting the approximate Green's functions into the Kirchhoff scattering integral. Numerical examples for a transversely isotropic medium above a horizontal reflector and for a structurally complex acoustic model with a salt body confirm the accuracy of the method.

INTRODUCTION

Attenuation analysis may provide seismic attributes sensitive to the physical properties of the subsurface. Reliable attenuation measurements have become feasible with acquisition of high-quality reflection and borehole data.

A prerequisite for estimating attenuation coefficients from seismic data is accurate and efficient modeling of wave propagation in heterogeneous attenuative media. Attenuation makes the stiffness tensor complex, which leads to amplitude decay along seismic rays and velocity dispersion. In the presence of attenuation, the stress tensor is obtained by convolving the time-domain stiffness tensor (called the relaxation tensor) with the strain tensor (Carcione, 1990), which complicates finite-difference modeling of wave propagation in the time domain. Further, simulation of a frequency-independent quality factor (constant-Q model, e.g., Kjartannson, 1979) requires superimposing various relaxation mechanisms (Xu and McMechan, 1998; Ruud and Hestholm, 2005) — a costly operation for finite-difference modeling. The approach based on the Fourier pseudospectral method proposed by Carcione (2010) avoids the computation of relaxation functions, but it is restricted to viscoacoustic media. Although the reflectivity method (Schmidt and Tango, 1986) can be used to calculate exact synthetic seismograms, the model has to be composed of horizontal, homogeneous layers.

A computationally fast alternative is ray tracing, which can generate asymptotic Green's functions in elastic and attenuative media (Červený, 2001). The so-called *complex ray theory* developed for attenuative models treats ray trajectories and parameters computed along the ray as complex quantities (Thomson, 1997; Hanyga and Seredyńska, 2000). However, numerical implementation of the complex ray theory in seismic modeling is difficult. Ray tracing in attenuative media can also be performed using perturbation methods, which involve computation of rays in a reference elastic medium with the influence of attenuation included as a perturbation along the ray (Gajewski and Pšenčik, 1992; Červený and Pšenčik, 2009; Shekar and Tsvankin, 2012).

Synthetic seismograms of reflected waves in heterogeneous media can be efficiently computed using the Kirchhoff scattering integral (Chapman, 2004). However, this method typically requires two-point ray tracing, which can produce inaccurate results for multivalued traveltimes (multipathing). Alternatively, the asymptotic Green's functions required in the Kirchhoff scattering integral can be found by summation of Gaussian beams (Červený, 2001; Bleistein, 2008). Gaussian-beam summation eliminates the need for two-point ray tracing and can accurately handle multipathing. It can also produce finite-frequency sensitivity kernels for amplitude inversion (Yomogida and Aki, 1987). Liu and Palacharla (2010) show that using Gaussian beams to perform Q-compensating Kirchhoff migration can better restore the amplitude and frequency content of images than single-arrival Kirchhoff imaging.

Here, we present a methodology for computing 2.5D ray synthetic seismograms from attenuative anisotropic media. First, we

Manuscript received by the Editor 19 November 2013; revised manuscript received 29 April 2014; published online 16 September 2014.
[1]Formerly Colorado School of Mines, Center for Wave Phenomena, Golden, Colorado, USA; presently Indian Institute of Technology Bombay, Department of Earth Sciences, Powai, Mumbai, India. E-mail: bshekar@iitb.ac.in.
[2]Colorado School of Mines, Center for Wave Phenomena, Department of Geophysics, Golden, Colorado, USA. E-mail: ilya@mines.edu.

describe the Kirchhoff scattering integral for purely elastic models and show how it should be modified in the presence of attenuation. Then, we review the method of summation of Gaussian beams and its application to computation of the asymptotic "two-point" Green's functions in attenuative media. Finally, the algorithm is implemented for heterogeneous transversely isotropic (TI) media and its accuracy is illustrated with numerical examples.

METHODOLOGY

Kirchhoff scattering integral

Suppose the wavefield is excited by a point impulsive force located at $\mathbf{x}^s$ and aligned with the x_k-axis, and the receiver is located at $\mathbf{x}^r$. The nth-component of the displacement field reflected from surface Σ is given in the frequency domain by (Červený, 2001)

$$G_{nk}(\mathbf{x}^r,\mathbf{x}^s,\omega)=-i\omega\int_\Sigma \mathcal{W}_{iq}(\mathbf{x}')G_{in}(\mathbf{x}',\mathbf{x}^s,\omega)G_{qk}(\mathbf{x}',\mathbf{x}^r,\omega)\mathrm{d}\Sigma, \tag{1}$$

where $\mathbf{x}'$ are points on surface Σ and the source- and receiver-side Green's functions [$G_{in}(\mathbf{x}',\mathbf{x}^s,\omega)$ and $G_{qk}(\mathbf{x}',\mathbf{x}^r,\omega)$, respectively] are computed for a smoothed medium. Throughout this paper, lowercase Roman indices take values from one to three and Einstein summation convention is implied. The weighting function $\mathcal{W}_{iq}(\mathbf{x}')$ is represented as

$$\mathcal{W}_{iq}(\mathbf{x}') = a^{(1)}_{ijql}(n_j p^r_l - n_l p^s_j)(1+R), \tag{2}$$

where $a^{(1)}_{ijql}$ is the local density-normalized stiffness tensor in the medium immediately above the reflector, $\mathbf{n}$ is the normal to the reflector, $\mathbf{p}^s$ and $\mathbf{p}^r$ are the source- and receiver-side slowness vectors at the scattering point, respectively, and R is the angle-dependent reflection coefficient.

Equation 1 is valid for an arbitrary scattering surface, and all Green's functions have to be computed in 3D. However, if we assume that the medium properties do not vary in the x_2-direction, and the [x_1, x_3]-plane is a plane of symmetry, equation 1 can be rewritten in a 2.5D form. Then, the surface integral in equation 1 can be reduced to a line integral by the method of stationary phase (Bleistein, 1984). Following Bleistein (1986), we apply the stationary-phase method to obtain the 2.5D form of the integral in equation 1:

$$G_{nk}(\mathbf{x}^r,\mathbf{x}^s,\omega) = -i\sqrt{2\pi\omega} \times\int_{C,\,x_2=0}\frac{1}{\sqrt{\sigma}}\mathcal{W}_{iq}(\mathbf{x}')G_{in}(\mathbf{x}',\mathbf{x}^s,\omega)G_{qk}(\mathbf{x}',\mathbf{x}^r,\omega)\mathrm{d}s, \tag{3}$$

where the Green's functions are defined in 2.5D, the scatterer is reduced to the curve C that lies in the [x_1, x_3]-plane, ds is an elementary arclength along C, and function σ accounts for out-of-plane phenomena:

$$\sigma = \left[\frac{1}{\partial^2 T(\mathbf{x}',\mathbf{x}^s)/\partial x_2^2}+\frac{1}{\partial^2 T(\mathbf{x}',\mathbf{x}^r)/\partial x_2^2}\right]_{x_2=0}; \tag{4}$$

$T(\mathbf{x}',\mathbf{x}^s)$ is the traveltime from the source to the scatterer and $T(\mathbf{x}',\mathbf{x}^r)$ is the traveltime from the receiver to the scatterer. The second-order spatial derivatives of the traveltime functions may be calculated by dynamic ray tracing (Appendix A).

Equations 1–4 can be extended to attenuative media by making the stiffness tensor complex and replacing the elastic Green's functions with their viscoelastic counterparts. Although the reflection coefficient and slowness vector also become complex in attenuative media, we compute these quantities for the reference elastic medium. Unless attenuation is anomalously high, plane-wave reflection coefficients are not significantly distorted in attenuative media (Behura and Tsvankin, 2009b). Although the complex-valued slowness vectors at the reflector can somewhat change the weighting function defined in equation 2, they do not significantly contribute to the displacement computed from equation 3 because attenuation is a propagation phenomenon.

Asymptotic Green's function as a sum of Gaussian beams

Although the Green's functions in equation 3 can be computed by two-point ray tracing (Bulant, 1996), that method cannot accurately handle multipathing and requires a search for the ray connecting the source and receiver. A more rigorous approach to modeling asymptotic Green's functions involves summation of Gaussian beams (Červený, 2001). Here, we start with analysis of 2.5D elastic anisotropic Green's functions and then describe the modifications needed for extending the methodology to attenuative media.

The Green's function $\mathbf{G}(\mathbf{x}',\mathbf{x}^s,\omega)$ can be found as a sum of Gaussian beams (Červený, 2001):

$$G_{ik}(\mathbf{x}',\mathbf{x}^s,\omega) = \Phi(\theta_0)\int u_{ik}[R(\gamma+\theta_0)]\mathrm{d}\gamma, \tag{5}$$

where $u_{ik}[R(\gamma+\theta_0)]$ represents a single Gaussian beam concentrated around the central ray $R(\gamma+\theta_0)$ and $\Phi(\theta_0)$ is the angle-dependent weighting function. Suppose that ray $R(\theta_0)$ with the initial (at the source $\mathbf{x}_s$) take-off phase angle θ_0 with respect to the horizontal illuminates a point close to $\mathbf{x}'$ (Figure 1). The range of integration in equation 5 is then chosen to be symmetric over $\gamma=0$, and the Green's function is obtained by summation over a fan of beams centered around the phase angle θ_0. Note that θ_0 does not appear in the argument of the Green's function in equation 5 because θ_0 implicitly depends on $\mathbf{x}_s$ and $\mathbf{x}'$ (Figure 1).

Červený (2001) derives the weighting function $\Phi(\theta_0)$ for heterogeneous media by evaluating the Gaussian integral. However, that result is valid only for "regular ray regions" that do not include caustics. Alternatively, the weighting function may be calculated in an asymptotic sense (Bleistein, 2008). Although the asymptotic function $\Phi(\theta_0)$ for heterogeneous media is approximate, it remains stable even in regions with caustics. The asymptotic angle-dependent weighting function for anisotropic media is derived in Appendix B (equation B-9). In isotropic media, the weighting function is independent of angle.

To evaluate the contribution of the Gaussian beam centered around ray $R(\gamma+\theta_0)$ to $\mathbf{G}(\mathbf{x}',\mathbf{x}^s,\omega)$, we consider point $\mathbf{x}''$ closest to $\mathbf{x}'$ on $R(\gamma+\theta_0)$ (Figure 1). Then, the contribution $u_{ik}[R(\gamma+\theta_0)]$ to $\mathbf{G}(\mathbf{x}',\mathbf{x}^s,\omega)$ is (Červený and Pšenčík, 2010)

$$u_{ik}(\mathbf{x}', \mathbf{x}^s, \omega) = g_i(\mathbf{x}'')g_k(\mathbf{x}'') \times \frac{1}{4\pi\sqrt{c(\mathbf{x}^s)c(\mathbf{x}'')}} \frac{1}{\sqrt{\det \tilde{\mathbf{W}}(\mathbf{x}'', \mathbf{x}^s)}} e^{-i\omega\tilde{T}(\mathbf{x}'', \mathbf{x}^s)}, \quad (6)$$

where the angle-dependent P-wave phase velocity corresponding to the ray $R(\gamma + \theta_0)$ at the locations $\mathbf{x}^s$ and $\mathbf{x}''$ is represented by $c(\mathbf{x}^s)$ and $c(\mathbf{x}'')$, respectively, $\mathbf{g}$ is the polarization vector, and $\tilde{T}(\mathbf{x}', \mathbf{x}^s)$ is the complex traveltime (Červený and Pšenčík, 2010):

$$\tilde{T}(\mathbf{x}', \mathbf{x}^s) = T(\mathbf{x}'', \mathbf{x}^s) + (\mathbf{x}' - \mathbf{x}'')^T \mathbf{p}[R(\gamma + \theta_0)] + \frac{1}{2}(\mathbf{x}' - \mathbf{x}'')^T \tilde{\mathbf{M}}^x (\mathbf{x}' - \mathbf{x}''), \quad (7)$$

where the superscript T denotes the transpose, $\mathbf{p}$ is the slowness vector corresponding to the ray $R(\gamma + \theta_0)$, and $\tilde{\mathbf{M}}^x$ is the complex-valued matrix of the second traveltime derivatives found by transforming the matrix $\tilde{\mathbf{M}}$ defined in Appendix A (equation A-15) to the Cartesian coordinates (Červený and Pšenčík, 2010). The matrix $\tilde{\mathbf{W}}(\mathbf{x}'', \mathbf{x}^s)$ depends on the initial value $\tilde{\mathbf{M}}^0$ of $\tilde{\mathbf{M}}$:

$$\tilde{\mathbf{W}}(\mathbf{x}'', \mathbf{x}^s) = \mathbf{Q}_1(\mathbf{x}'', \mathbf{x}^s) + \mathbf{Q}_2(\mathbf{x}'', \mathbf{x}^s)\tilde{\mathbf{M}}^0, \quad (8)$$

where $\mathbf{Q}_1$ and $\mathbf{Q}_2$ are computed by dynamic ray tracing in ray-centered coordinates (see Appendix A). Matrix $\tilde{\mathbf{M}}^0$ is given by equation A-16:

$$\tilde{\mathbf{M}}^0 = \frac{i}{l\,\omega^2}\mathbf{I}, \quad (9)$$

where $\mathbf{I}$ is the identity matrix and l represents the initial beam width. The choice of l and the sampling of the parameter γ are discussed in the next section.

If the medium is attenuative, equation 5 can be adapted to obtain the viscoelastic Green's function $\mathbf{G}^{\text{att}}(\mathbf{x}', \mathbf{x}^s, \omega)$ (Červený, 1985):

$$G^{\text{att}}_{ik}(\mathbf{x}', \mathbf{x}^s, \omega) = \Phi(\theta_0) \int \mathbf{u}^{\text{att}}_{ik}[R(\gamma + \theta_0)]\mathrm{d}\gamma. \quad (10)$$

The weighting function $\Phi(\theta_0)$ remains unchanged from that in elastic media, whereas $\mathbf{u}^{\text{att}}_{ik}(R)$ becomes

$$\mathbf{u}^{\text{att}}_{ik}[R(\gamma + \theta_0)] = \mathbf{u}_{ik}[R(\gamma + \theta_0)]e^{-\omega t^*(\mathbf{x}', \mathbf{x}^s)}, \quad (11)$$

where $\mathbf{u}_{ik}[R_0(\gamma)]$ is computed for the reference elastic medium and $t^*(\mathbf{x}', \mathbf{x}^s)$ is a real-valued quantity called the *dissipation factor* (Gajewski and Pšenčík, 1992), which accounts for the attenuation-induced amplitude decay along the central ray. The factor t^* can be calculated using perturbation methods (Červený and Pšenčík, 2009; Shekar and Tsvankin, 2012).

Implementation

The initial beam width for Gaussian beams in anisotropic media can be chosen as (Alkhalifah, 1995)

$$l = \frac{V_{\text{avg}}}{f_{\min}}, \quad (12)$$

where V_{avg} represents the average of the horizontal and vertical phase velocities over the entire model and $f_{\min}$ is the lowest frequency of interest.

Next, we discuss the sampling of parameter γ in the summation of Gaussian beams (equations 5 and 10). Following Hill (1990), Hale (1992) derives the following expression for the sampling in the horizontal slowness p_x:

$$\mathrm{d}p_x = \frac{1}{6l\sqrt{f_{\min} f_{\max}}}, \quad (13)$$

where $f_{\max}$ is the highest frequency of interest. In TI media, the velocity c is a function of angle, and the horizontal slowness can be expressed as

$$p_x = \frac{\cos(\gamma + \theta_0)}{c(\gamma + \theta_0)}. \quad (14)$$

Using equations 13 and 14, the sampling $\mathrm{d}\gamma$ can be related to $\mathrm{d}p_x$ by

$$|\mathrm{d}p_x| = \left| \frac{\sin(\gamma + \theta_0)}{c(\gamma + \theta_0)} + \frac{\cos(\gamma + \theta_0)}{c^2(\gamma + \theta_0)} \frac{\mathrm{d}c(\gamma + \theta_0)}{\mathrm{d}\gamma} \right|_{\gamma = 0} |\mathrm{d}\gamma| = \left| \frac{\sin\,\theta_0}{c(\theta_0)} + \frac{\cos\,\theta_0}{c^2(\theta_0)} \frac{\mathrm{d}c(\gamma + \theta_0)}{\mathrm{d}\gamma} \right| |\mathrm{d}\gamma|; \quad (15)$$

the derivative $\mathrm{d}c(\gamma + \theta_0)/\mathrm{d}\gamma$ is evaluated at $\gamma = 0$.

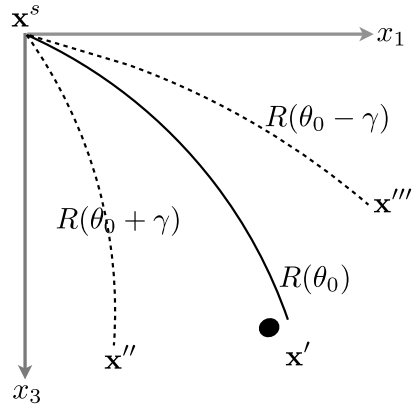

Figure 1. Diagram illustrating the computation of the Green's function as a sum of Gaussian beams. The source exciting the Green's function is at point $\mathbf{x}^s$, and the receiver location is $\mathbf{x}'$. The ray $R(\theta_0)$ defined by the take-off phase angle θ_0 (generally different from the ray angle) with respect to the horizontal axis illuminates a point close to $\mathbf{x}'$. The points $\mathbf{x}''$ and $\mathbf{x}'''$, located on rays $R(\theta_0 + \gamma)$ and $R(\theta_0 - \gamma)$, respectively, are the closest points to $\mathbf{x}'$. The Green's function is obtained as a summation of Gaussian beams centered around each ray in the range from $R(\theta_0 - \gamma)$ to $R(\theta_0 + \gamma)$.

We calculate the reflected wavefields in attenuative heterogeneous media using equation 3 with the source-to-scatterer and scatterer-to-receiver Green's functions obtained using equations 5 and 6. The Gaussian beams in attenuative media are computed from equation 11. The ray tracing is performed in the frequency domain and parametrized by the real-valued stiffness tensor for the reference elastic medium and by the complex-valued stiffness tensor for the attenuative medium. The beams are constructed in the reference elastic medium, and the dissipation factor t^* is found as a perturbation along the central ray (Červený and Pšenčik, 2009; Shekar and Tsvankin, 2012). The weighting function $\Phi(\theta_0)$ for the summation of Gaussian beams is also calculated in the reference elastic medium. Likewise, the weighting functions σ and $\mathcal{W}_{iq}$ for the Kirchhoff integral (equation 3) are found from the quantities stored during the modeling of Gaussian beams in the reference elastic medium. For TI models, the reflection coefficient R in equation 2 is obtained from the weak-contrast, weak-anisotropy approximation for P-waves presented by Rüger (1997).

SYNTHETIC TESTS

First, we verify the accuracy of the Gaussian beam summation method in constructing the asymptotic Green's function in unbounded media. Table 1 lists the velocity and attenuation parameters for the two TI models used to test the Gaussian beam summation. Model 1 is homogeneous, and model 2 has a vertical gradient (k_z) in the symmetry-direction (vertical) P-wave velocity V_{P0}:

$$V_{P0}(z) = V_{P0}(0)\Big(1 + k_z z\Big). \tag{16}$$

Figure 2 compares the Green's function computed from perturbation ray theory (Červený and Pšenčik, 2009; Shekar and Tsvankin, 2012) and Gaussian beam summation (equation 11) for the two TI models. Note that equation 11 also uses perturbation ray theory to incorporate the contribution of attenuation. The two functions are close to each other for model 1 (Figure 2a, 2c, and 2e), whereas there is a noticeable deviation in the amplitudes for model 2 (Figure 2b, 2d, and 2f), which has a vertical velocity gradient. The asymptotic weighting function $\Phi(\theta_0)$ (equation B-9) is derived for a homogeneous, anisotropic medium with the medium parameters corresponding to the surface. The strong vertical velocity gradient combined with the velocity anisotropy is responsible for the amplitude error for model 2. The displacement computed from the beam summation exhibits a phase distortion because only a finite number of Gaussian beams is taken into account.

Table 1. Parameters of two VTI models used to test the accuracy of Gaussian beam summation. Model 2 is vertically heterogeneous with a constant gradient (k_z) in V_{P0}. The attenuation-anisotropy parameters ϵ_Q and δ_Q are defined in Zhu and Tsvankin (2006) and Tsvankin and Grechka (2011, chapter 8).

	Model 1	Model 2
V_{P0} (km/s)	3.00	3.00
V_{S0} (km/s)	1.50	1.50
k_z (1/km)	0.0	1.50
ϵ	0.40	0.40
δ	0.25	0.25
Q_{P0}	10	10
Q_{S0}	10	10
ϵ_Q	−0.40	−0.40
δ_Q	−0.25	−0.25

Next, the Gaussian-beam summation method is applied to a structurally complicated but isotropic 2D model. Figure 3a displays a P-wave velocity slice extracted from the SEG/EAGE acoustic salt model (Aminzadeh et al., 1996); a smooth version of the velocity model used to perform ray tracing is shown in Figure 3b. The smoothing was performed over slowness using Seismic Un*x (SU) (Stockwell, 1999) function "smooth3d," which uses a damped least-squares approach to preserve traveltimes. Rays traced from a source at (6.72 km, 0.10 km) exhibit shadow zones and multipathing because of the vertical and lateral velocity variations and, particularly, due to the presence of the salt body (Figure 3b).

Figure 4 shows the seismograms of pressure at a depth of 3 km generated by a source placed at (6.72 km, 0.10 km) in the model from Figure 3. The section in Figure 4a was computed with the SU finite-difference function "sufdmod2" for the model in Figure 3a. The section in Figure 4b was obtained by Gaussian-beam summation method for 2D acoustic media (Hill, 1990; Červený, 2001; Bleistein, 2008) applied to the smoothed model in Figure 3b. We then introduced isotropic attenuation in the model with a spatially invariant P-wave quality factor $Q_P = 10$. The contribution of attenuation was incorporated by combining perturbation ray theory with beam summation, as discussed above; the resulting traces are plotted in Figure 4c. Predictably, the waveforms in Figure 4c are wider due to the influence of attenuation, which suppresses high frequencies.

To gain insight into the performance of Gaussian-beam summation, in Figure 5 we analyze individual traces from Figure 4a and 4b extracted for the horizontal coordinate x in the range 5–9 km, which corresponds to the region with the most significant energy in Figure 4a. Because the Gaussian-beam summation was performed for a smooth model, it somewhat distorts the geometric spreading for the model in Figure 3a. Moreover, the ray tracing used in the summation of beams does not take into account reflection/transmission coefficients and multiple scattering. Hence, the beam-summation technique inevitably produces some errors in amplitudes. Also, beam summation cannot reconstruct side lobes (or coda) visible in the traces obtained by the finite-difference method (Figure 5) because the coda is generated mostly by internal scattering inside the salt body.

However, in the parts of the model with a good ray coverage (e.g., for $5 < x < 9$ km; see Figure 3b), the main lobes of the traces produced by the finite-difference and beam-summation methods almost coincide, except for a slight time shift caused by the smoothed velocity model in beam summation (Figure 5b and 5c). For regions with poor ray coverage, the beam-summation method yields traces with multiple lobes absent on the finite-difference seismograms. These errors are already visible in Figure 5a and 5d, and become larger for $x < 5$ km and $x > 9$ km. If the

ray density is low, the Gaussian beams centered on successive rays are out of phase and do not sum coherently.

The accuracy of the algorithm in accounting for attenuation can be verified by computing the attenuation coefficients from the modeled data. We apply the spectral-ratio method (Johnston and Toksöz, 1981; Zhu et al., 2007), which operates with isolated events, to the traces in Figure 4c. Because the attenuation function for this model is spatially invariant, the slope of the logarithmic

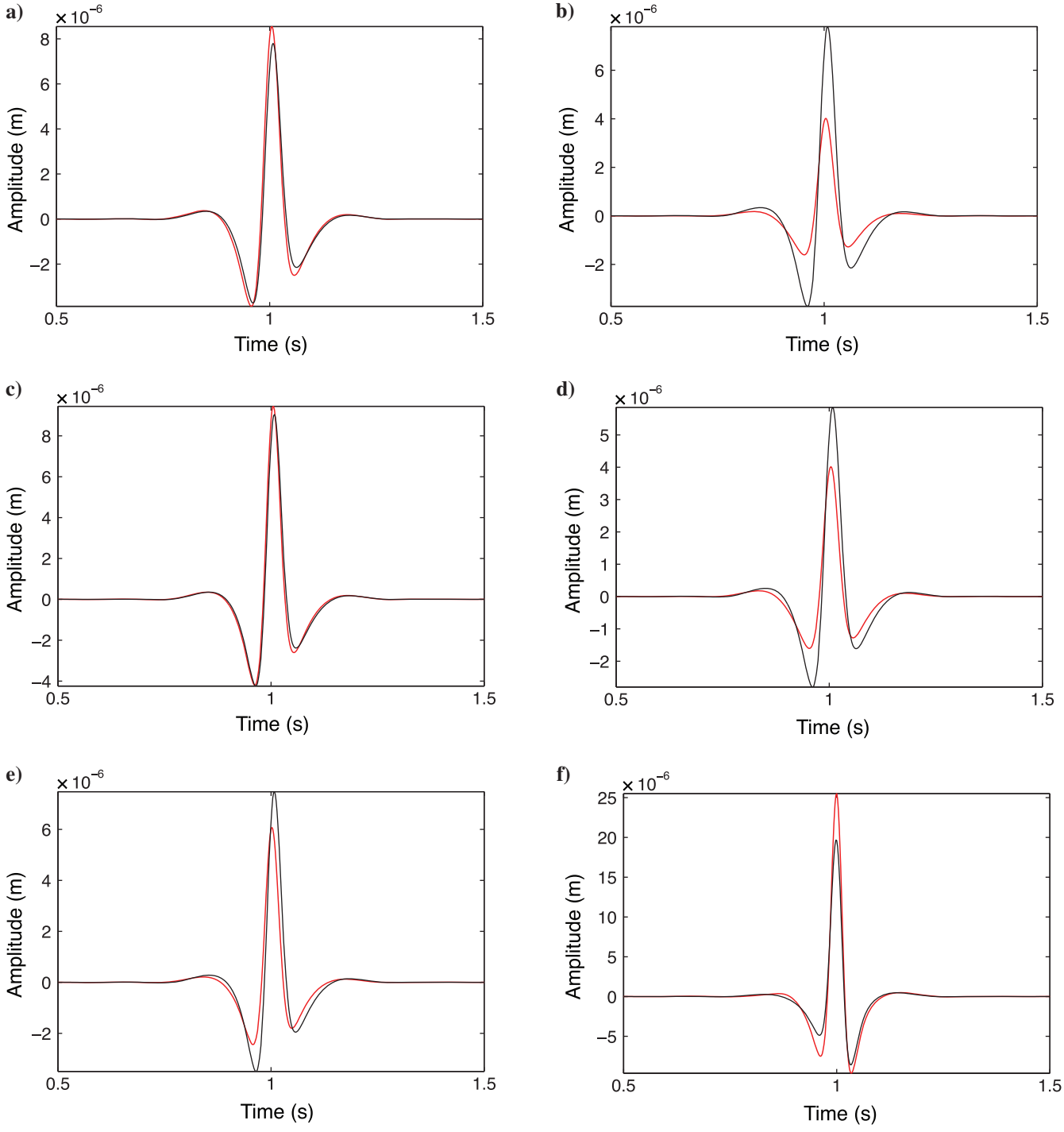

Figure 2. Comparison of the vertical displacement component computed using the Gaussian-beam summation method (red curves) and perturbation ray theory (black) for model 1 (a, c, and e) and model 2 (b, d, and f) from Table 1. The group angle with the vertical is (a and b) 0°, (c and d) 30°, and (e and f) 60°; the propagation time is 1 s. The wavefield is excited by a vertical point force; the source signal is a Ricker wavelet with a central frequency of 30 Hz.

spectral ratio obtained by dividing the amplitude spectrum of an event and the source spectrum yields the product of the traveltime t along the raypath and the normalized P-wave attenuation coefficient $\mathcal{A}_P = 1/(2Q_P)$ (Behura and Tsvankin, 2009a). The estimated attenuation coefficient is close to the actual one ($\mathcal{A}_P = 0.05$) for a range of x-values, but there are deviations for $x < 5.5$ km and $x > 8.5$ km (Figure 6) caused by the relatively sparse ray coverage in these regions (Figure 3b).

In Figure 7, we test the accuracy of the Kirchhoff scattering integral combined with Gaussian-beam summation in generating reflection data for VTI media. Table 2 displays the velocity and attenuation parameters for a model that includes two homogeneous VTI layers separated by a horizontal reflector. The exact reflected wavefield (Figure 7a) was computed with the reflectivity method (Mallick and Frazer, 1990). The displacement obtained from the Kirchhoff scattering integral (Figure 7b) almost coincides with the exact solution, except for a small phase distortion (Figure 7c and 7d).

DISCUSSION

The outlined method involves several approximations. The Kirchhoff scattering integral itself is an asymptotic solution that ignores multiple scattering (Chapman, 2004). The method of summation of Gaussian beams is limited to computing asymptotic Green's functions in smooth media and does not account for multiples, scattering losses, and reflection/transmission coefficients.

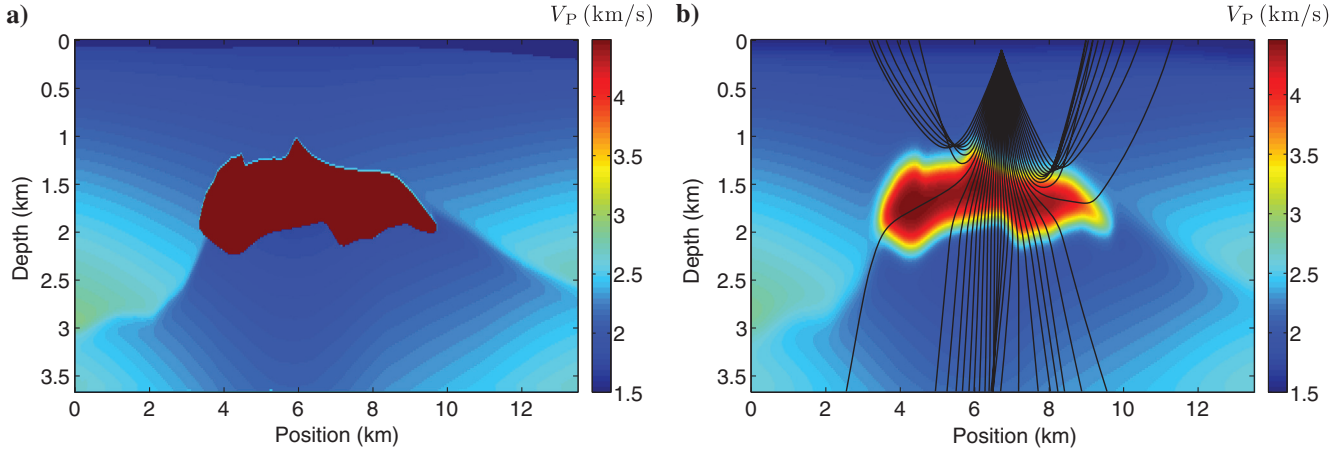

Figure 3. (a) 2D velocity slice from the SEG/EAGE salt model. (b) The smoothed version of the model from panel (a) used for ray tracing. A fan of rays originating from a shot with the horizontal position of 6.72 km and at a depth of 0.10 km with a 4° increment in the take-off angle is plotted in black.

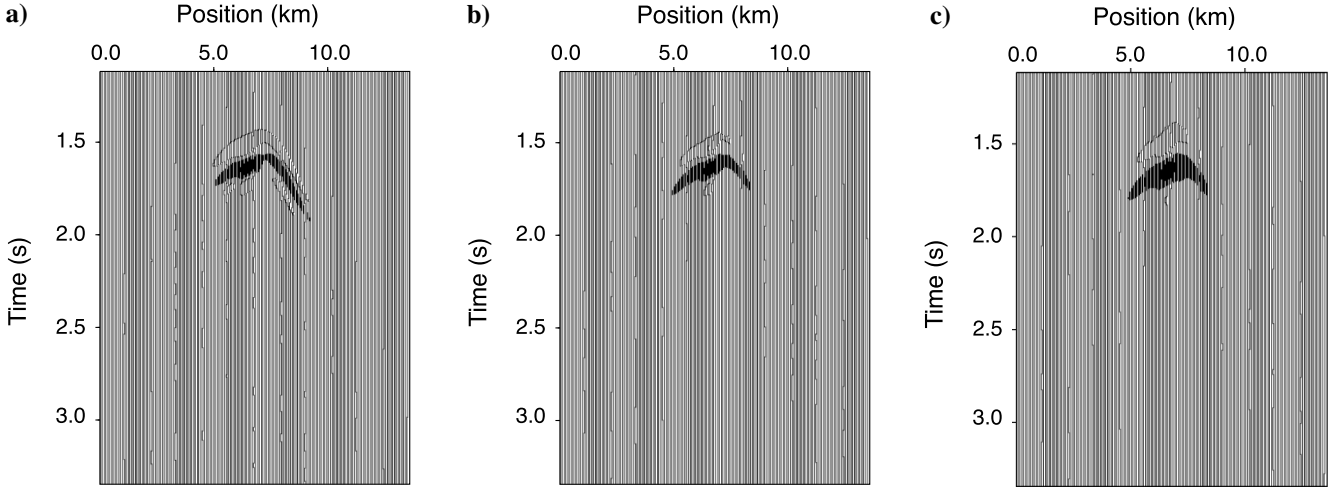

Figure 4. Pressure field at depth of 3.0 km from a shot at (6.72 km, 0.10 km) computed with (a) finite-differences for the nonattenuative model in Figure 3a and with the Gaussian-beam summation for the model in Figure 3b (b) without attenuation and (c) with a spatially invariant value of $Q_P = 10$.

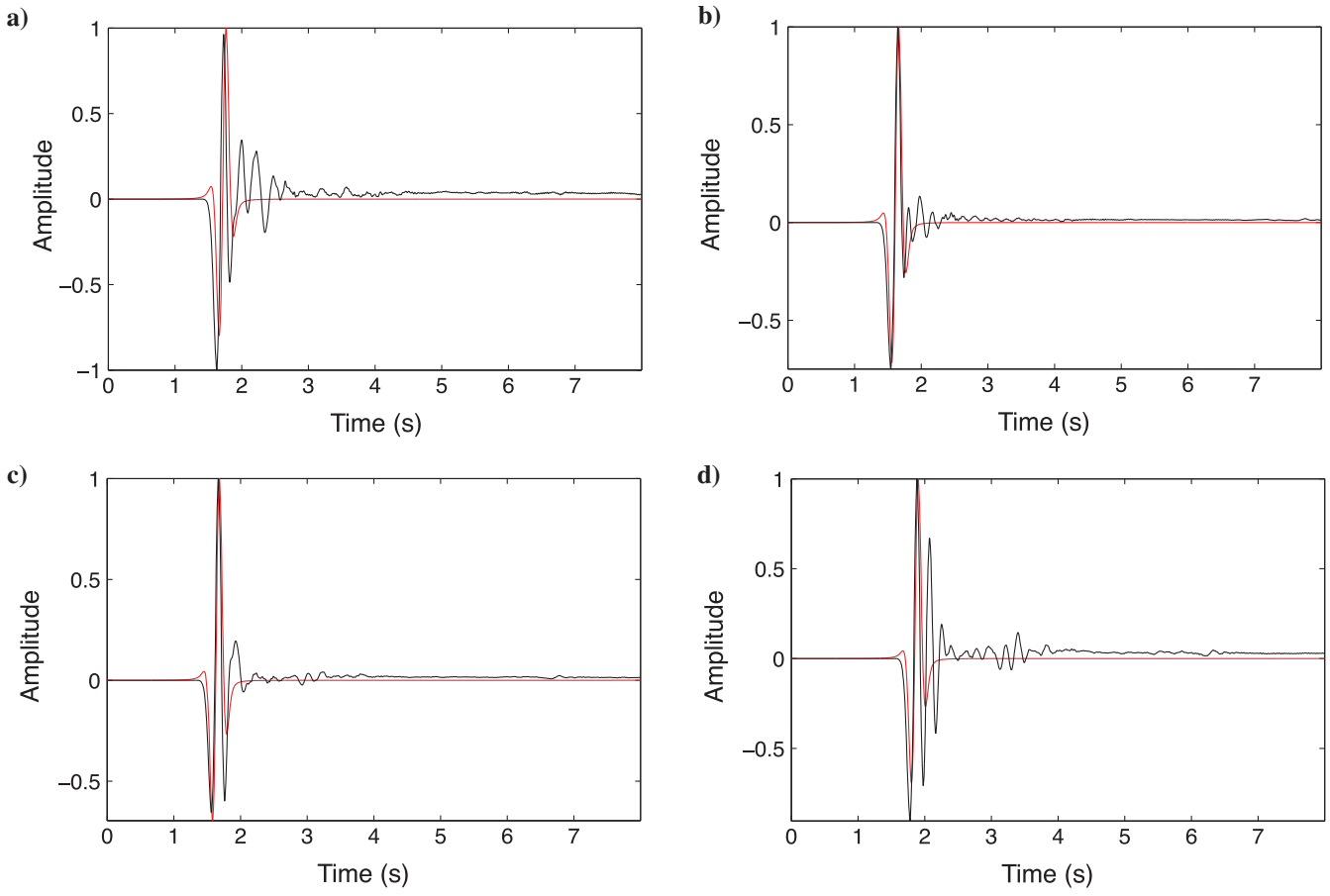

Figure 5. Traces (normalized by the maximum amplitude) from Figure 4a (produced by finite differences; black lines) and Figure 4b (produced by Gaussian-beam summation; red) at horizontal positions of (a) 5, (b) 6, (c) 8, and (d) 9 km.

The scope of this paper is restricted to P-waves, and the accuracy of modeling mode conversions has not been studied. The influence of attenuation is modeled using perturbation theory, which is valid for weakly dissipative media. Numerical examples illustrating the accuracy of the perturbation approach can be found in Shekar and Tsvankin (2012).

It is well known that the presence of attenuation leads to velocity dispersion, which causes phase distortions of seismic signals. Although this paper does not treat velocity dispersion explicitly, the method can be modified by introducing a complex-valued dissipation factor with the real part computed from the perturbation approach and the imaginary part obtained from a dispersion relation. However, although dispersion relations have been extensively studied for acoustic media (Futterman, 1962; Liu et al., 1976; Kjartannson, 1979), few studies are focused on anisotropic models (e.g., Jakobsen and Chapman, 2009).

In migration algorithms with Q-compensation, regularization is necessary to mitigate the exponential amplitude increase at high frequencies (Zhang et al., 2010). Likewise, amplitudes may go to zero during forward modeling in attenuative media, and it might be necessary to add constraints to our modeling algorithm. Finally, as shown by the numerical testing above, the accuracy of Green's functions obtained from Gaussian-beam summation for structurally complicated models varies with ray coverage. This limitation of initial-value ray tracing may be overcome by using wavefront-construction techniques that improve illumination.

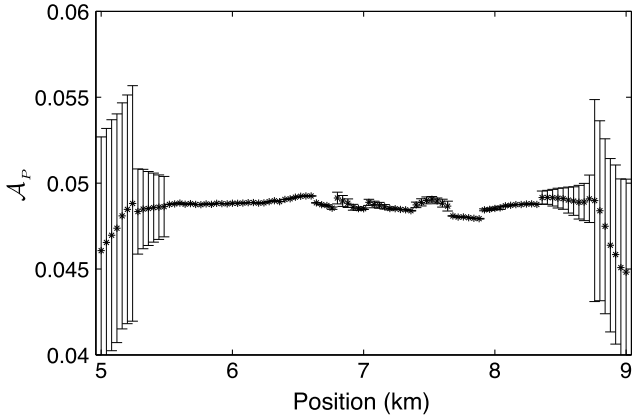

Figure 6. P-wave attenuation coefficient $\mathcal{A}_P$ computed using the traces from Figure 4c. The error bars mark two standard deviations in $\mathcal{A}_P$ (95% confidence intervals).

Table 2. Parameters of a two-layer VTI model used to test the Kirchhoff scattering integral.

	Layer 1	Half-space
Thickness (km)	2.00	—
V_{P0} (km/s)	3.00	3.20
V_{S0} (km/s)	1.50	1.60
ϵ	0.20	0.10
δ	0.10	0.05
Q_{P0}	10	100
Q_{S0}	10	100
ϵ_Q	0.0	0.0
δ_Q	0.75	0.0

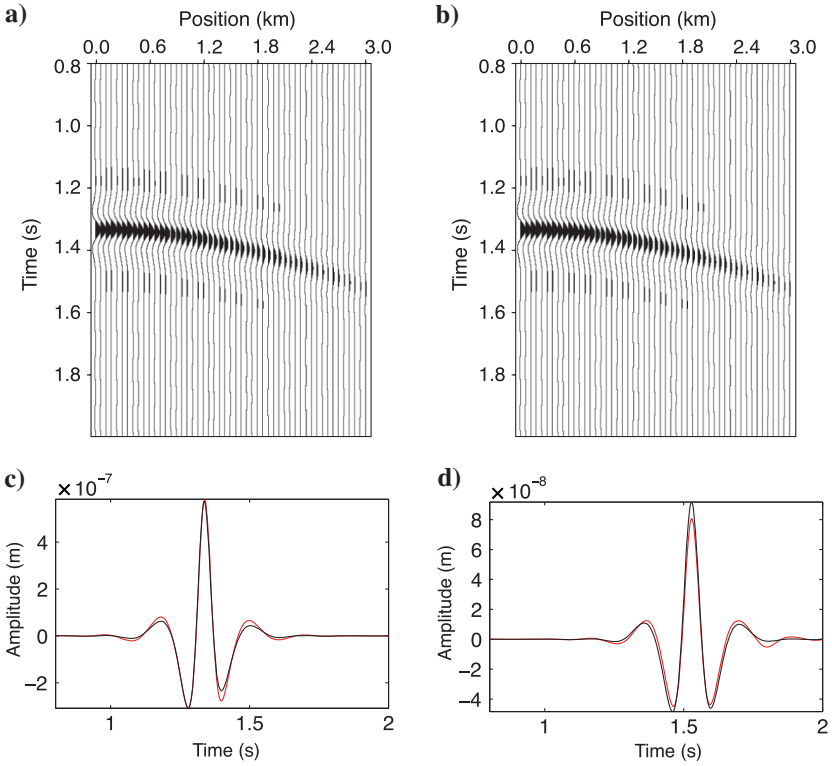

Figure 7. Vertical displacement for the model in Table 2 generated using (a) the reflectivity method and (b) the Kirchhoff scattering integral. The wavefield is excited and recorded on top of the model. The source is a vertical force at a horizontal position of 0 km, and the receivers are placed on the surface between 0 and 3 km with a 25 m increment. The source signal is a Ricker wavelet with a central frequency of 10 Hz. The traces from the reflectivity method (black) and the Kirchhoff scattering integral (red) for the receiver at (c) 0 and (d) 3 km.

CONCLUSIONS

We introduced a ray-based methodology for computing synthetic seismograms of reflected waves from attenuative anisotropic media. The wavefield is generated with the Kirchhoff scattering integral that includes 2.5D asymptotic Green's functions. Summation of Gaussian beams is used to calculate the Green's functions in the reference purely elastic, anisotropic medium. The contribution of attenuation to Gaussian beams is accounted for by perturbation ray theory.

The accuracy of the Gaussian-beam summation method in producing Green's functions was verified for a highly attenuative TI layer and for a structurally complex acoustic model containing a salt body. In regions with sufficient ray coverage, the waveforms from the Gaussian-beam summation method compare well with the finite-difference solution. The attenuation coefficient estimated by the spectral-ratio method from the data generated with our method is generally close to the actual value. Some distortions in the reconstructed attenuation coefficients are caused by insufficient ray coverage related to the heterogeneity of the velocity field.

The performance of the algorithm was also analyzed by comparing the wavefield produced by the Kirchhoff scattering integral for a horizontally layered VTI medium with exact seismograms computed using the reflectivity method. These examples confirm that the proposed technique adequately models P-wave reflections even in the presence of strong anisotropic attenuation. The displacements obtained by our method, however, exhibit minor phase distortions due to a finite number of beams used to generate the Green's functions.

ACKNOWLEDGMENTS

We are grateful to the members of the A(nisotropy)-Team of the Center for Wave Phenomena (CWP), Colorado School of Mines, for fruitful discussions. We are grateful to associate editor L. Lines, S. Gray, and two anonymous reviewers for their constructive suggestions. This work was supported by the Consortium Project on Seismic Inverse Methods for Complex Structures at CWP.

APPENDIX A

DYNAMIC RAY TRACING AND GAUSSIAN BEAMS IN ANISOTROPIC MEDIA

In this appendix, we briefly review dynamic ray tracing in anisotropic media and introduce the quantities necessary for the construction of Gaussian beams.

The eikonal equation in elastic, anisotropic, heterogeneous media can be written as (Červený, 2001)

$$G(x_i, p_i) = 1, \tag{A-1}$$

where x_i are the spatial coordinates and p_i are the components of the slowness vector. The solutions of equation A-1 represent the eigenvalues of the Christoffel equation:

$$\det[\Gamma_{ik} - G\,\delta_{ik}] = 0, \tag{A-2}$$

where $\Gamma_{ik} = a_{ijkl} p_j p_l$ are the components of the Christoffel matrix and a_{ijkl} form the density-normalized stiffness tensor.

The kinematic ray-tracing equations are given by (Červený, 2001)

$$\frac{\mathrm{d}x_i}{\mathrm{d}\tau} = \frac{1}{2}\frac{\partial G}{\partial p_i} \tag{A-3}$$

and

$$\frac{\mathrm{d}p_i}{\mathrm{d}\tau} = \frac{1}{2}\frac{\partial G}{\partial x_i}, \tag{A-4}$$

where τ represents the traveltime (eikonal) along the ray.

The dynamic ray-tracing system in ray-centered coordinates can be represented as (Červený, 2001)

$$\frac{\mathrm{d}P_{NI}}{\mathrm{d}\tau} = -C_{NM}Q_{MI} - D_{NM}P_{MI} \tag{A-5}$$

and

$$\frac{\mathrm{d}Q_{NI}}{\mathrm{d}\tau} = A_{NM}Q_{MI} + B_{NM}P_{MI}, \tag{A-6}$$

where the indices N, M, and I vary from one to two. Explicit expressions for matrices $\mathbf{A}$, $\mathbf{B}$, $\mathbf{C}$, and $\mathbf{D}$ can be found in Červený (2001). The matrices P_{MI} and Q_{NI} are defined as

$$P_{NI} = \frac{\partial p_N}{\partial \gamma_I} \tag{A-7}$$

and

$$Q_{NI} = \frac{\partial q_N}{\partial \gamma_I}, \tag{A-8}$$

where γ_I is a certain "ray parameter" (e.g., the phase angle of the ray), q_N are the coordinates tangent to the wavefront, and p_N denotes the slowness vector in the ray-centered coordinate system:

$$p_N = \frac{\partial \tau}{\partial q_N}. \tag{A-9}$$

The columns of $\mathbf{P}$ are unit vectors tangent to the wavefront, and the columns of $\mathbf{Q}$ are unit vectors tangent to the slowness surface. The 3×3 matrices $\mathbf{P}^x$ and $\mathbf{Q}^x$ correspond to $\mathbf{P}$ and $\mathbf{Q}$ in Cartesian coordinates (Červený, 2001):

$$P^x_{ik} = \frac{\partial p_i}{\partial \gamma_k} \tag{A-10}$$

and

$$Q^x_{ik} = \frac{\partial x_i}{\partial \gamma_k}. \tag{A-11}$$

The first two columns of $\mathbf{P}^x$ and $\mathbf{Q}^x$ have the same meaning as the two columns of $\mathbf{P}$ and $\mathbf{Q}$, respectively, whereas $P^x_{i3} = \mathrm{d}p_i/\mathrm{d}\tau$ and $Q^x_{i3} = \mathrm{d}x_i/\mathrm{d}\tau$.

The solutions of equations A-5 and A-6 for the plane-wave initial conditions ($\mathbf{Q} = \mathbf{I}$, $\mathbf{P} = 0$; $\mathbf{I}$ is the identity matrix) are denoted by $\mathbf{Q}_1$ and $\mathbf{P}_1$, and for the point-source initial conditions ($\mathbf{Q} = 0$, $\mathbf{P} = \mathbf{I}$) by $\mathbf{Q}_2$ and $\mathbf{P}_2$.

It is convenient to introduce the real-valued matrix $\mathbf{M}$ of the second-order traveltime derivatives:

$$\mathbf{M} = \mathbf{P}\,\mathbf{Q}^{-1}. \tag{A-12}$$

As discussed in the main text (equation 7), the matrix $\mathbf{M}$ is used for computing the paraxial traveltime. For the point-source initial conditions,

$$\mathbf{M} = \mathbf{P}_2\mathbf{Q}_2^{-1}. \tag{A-13}$$

A Gaussian beam can be constructed using the solution of equations A-5 and A-6 with complex-valued initial conditions (Bleistein, 2008):

$$\mathbf{Q} = \frac{l\,\omega^2}{c_0}\mathbf{I}, \qquad \tilde{\mathbf{P}} = \frac{i}{c_0}\mathbf{I}, \tag{A-14}$$

where l is the initial value of the beam width, ω is the angular frequency, and c_0 is the phase velocity at the source location corresponding to the take-off phase angle. The matrix $\mathbf{M}$ becomes complex-valued:

$$\tilde{\mathbf{M}} = [\mathbf{P}_1 + \tilde{\mathbf{M}}_0\,\mathbf{P}_2][\mathbf{Q}_1 + \tilde{\mathbf{M}}_0\mathbf{Q}_2]^{-1}. \tag{A-15}$$

The initial value of $\tilde{\mathbf{M}}$ is

$$\tilde{\mathbf{M}}^0 = \frac{i}{l\,\omega^2}\mathbf{I}. \tag{A-16}$$

The matrix $\tilde{\mathbf{M}}$ is used to construct the paraxial traveltime (equation 7). Because $\tilde{\mathbf{M}}$ is complex-valued, the traveltime is complex-valued as well, which leads to amplitude decay away from the central ray.

APPENDIX B

ASYMPTOTIC WEIGHTING FUNCTION Φ FOR 2.5D ANISOTROPIC MEDIA

In this section, we derive the weighting function $\Phi(\theta_0)$ for the summation of Gaussian beams. We assume that the medium properties do not vary in the x_2-direction, and the $[x_1, x_3]$-plane is a plane of symmetry; i.e., we treat the wave propagation in 2.5D. The analysis presented here is similar to that for isotropic media in Bleistein (2008).

Following Bleistein (2008), we consider equation 5 for a homogeneous anisotropic medium characterized by the medium properties at the source location $\mathbf{x}^s$. Substituting equation 6 into equation 5 (see the main text) for the summation of Gaussian beams yields

$$G_{ik}(\mathbf{x}', \mathbf{x}^s, \omega) = \Phi(\theta_0) \times \int g_i(\mathbf{x}'')g_k(\mathbf{x}'')\frac{1}{4\pi c(\mathbf{x}^s)}\frac{1}{\sqrt{\det \tilde{\mathbf{W}}(\mathbf{x}'', \mathbf{x}^s)}}e^{-i\omega\tilde{T}(\mathbf{x}'', \mathbf{x}^s)}\mathrm{d}\gamma. \tag{B-1}$$

The parameter γ represents the take-off phase angle measured with respect to the central ray $R(\theta_0)$, and the range of integration is chosen to be symmetric over θ_0 (Figure B-1). The ray corresponding to the phase angle $\gamma + \theta_0$ includes $\mathbf{x}''$, the point closest to $\mathbf{x}'$. The traveltime $\tilde{T}(\mathbf{x}'', \mathbf{x}^s)$ is given by

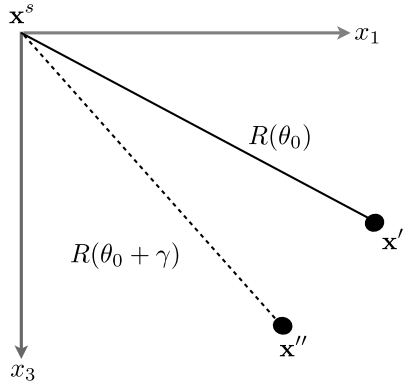

Figure B-1. Diagram illustrating the computation of the asymptotic weighting function $\Phi(\theta_0)$. The source exciting the Green's function is at point $\mathbf{x}^s$ and the receiver location is $\mathbf{x}'$. The ray $R(\theta_0)$ defined by the take-off phase angle θ_0 (generally different from the ray angle) with respect to the horizontal axis illuminates $\mathbf{x}'$. The closest point to $\mathbf{x}'$ on ray $R(\theta_0+\gamma)$ is denoted by $\mathbf{x}''$.

$$\tilde{T}(\mathbf{x}'',\mathbf{x}^s) = (\mathbf{x}'-\mathbf{x}^s)^T\,\mathbf{p}[R(\theta_0+\gamma)] + \frac{1}{2}(\mathbf{x}'-\mathbf{x}'')^T\,\tilde{\mathbf{M}}^x(\mathbf{x}'-\mathbf{x}''). \tag{B-2}$$

In the high-frequency approximation, the integral in equation B-1 can be evaluated using the method of steepest descent. Applying the saddle-point condition to the phase function $\psi = \tilde{T}(\mathbf{x}'',\mathbf{x}^s)$ leads to

$$\frac{\partial\psi}{\partial\gamma} = \frac{\partial\tilde{T}(\mathbf{x}'',\mathbf{x}^s)}{\partial\gamma} = 0. \tag{B-3}$$

Substituting equation B-2 into B-3, we find

$$\frac{\partial\tilde{T}(\mathbf{x}'',\mathbf{x}^s)}{\partial\gamma} = (\mathbf{x}'-\mathbf{x}^s)^T\left[\frac{\partial\mathbf{p}[R(\theta_0+\gamma)]}{\partial\gamma}\right] + \frac{1}{2}(\mathbf{x}'-\mathbf{x}'')^T\left[\frac{\partial\tilde{\mathbf{M}}^x}{\partial\gamma}\right](\mathbf{x}'-\mathbf{x}'')^T - \left[\frac{\partial\mathbf{x}'}{\partial\gamma}\right]^T\tilde{\mathbf{M}}^x(\mathbf{x}'-\mathbf{x}''). \tag{B-4}$$

Using equations A-10 and A-11, equation B-4 can be rewritten as

$$\frac{\partial\tilde{T}(\mathbf{x}'',\mathbf{x}^s)}{\partial\gamma} = (x_i'-x_i^s)P^x_{i1}[R(\theta_0+\gamma)]\,|\mathbf{p}[R(\theta_0+\gamma)]| + \frac{1}{2}(x_i{}'-x_i{}'')^T\left[\frac{\partial\tilde{M}^x_{ij}}{\partial\gamma}\right](x_j{}'-x_j{}'')^T - |\mathbf{x}'-\mathbf{x}''|\,Q^x_{i1}[R(\theta_0+\gamma)]\,\tilde{M}^x_{ij}(x_j{}'-x_j{}''). \tag{B-5}$$

Because the vectors formed by the first columns of $\mathbf{P}^x$ and $\mathbf{Q}^x$ are perpendicular to the slowness surface and the wavefront, respectively, the saddle-point condition is satisfied for $\mathbf{x}'=\mathbf{x}''$, i.e., for $\gamma=0$.

Next, it is necessary to evaluate the second derivative of the phase function ψ at the saddle point:

$$\left.\frac{\partial^2\psi}{\partial\gamma^2}\right|_{\gamma=0} = \left.\frac{\partial^2\tilde{T}(\mathbf{x}'',\mathbf{x}^s)}{\partial\gamma^2}\right|_{\gamma=0} = (x_i'-x_i^s)\left[\frac{\partial P^x_{i1}[R(\theta_0+\gamma)]}{\partial\gamma}\right]_{\gamma=0}|\mathbf{p}[R(\theta_0)]| + |\mathbf{x}'-\mathbf{x}''|^2\,Q^x_{i1}[R(\theta_0)]\left[\frac{\partial\tilde{M}^x_{ij}}{\partial\gamma}\right]_{\gamma=0}Q^x_{j1}[R(\theta_0)]. \tag{B-6}$$

Note that the matrices $\mathbf{P}^x$ and $\mathbf{Q}^x$ in equation B-6 are computed for the point-source initial conditions. The steepest-descent direction with respect to the real axis is defined by $(1/2)\,\arg(\partial^2\psi/\partial\gamma^2)|_{\gamma=0}$.

Equation B-1 reduces to

$$G_{ik}(\mathbf{x}',\mathbf{x}^s,\omega) = \sqrt{\frac{2\pi}{\omega}}\Phi(\theta_0)\,g_i(\mathbf{x}')g_k(\mathbf{x}')\frac{1}{4\pi c(\mathbf{x}^s)}\frac{1}{\sqrt{\det\tilde{\mathbf{W}}(\mathbf{x}',\mathbf{x}^s)}} \times\frac{1}{\sqrt{\partial^2\psi/\partial\gamma^2|_{\gamma=0}}}\exp(-i\omega\tilde{T}(\mathbf{x}',\mathbf{x}^s)). \tag{B-7}$$

The weighting function $\Phi(\theta_0)$ can be found by substituting the ray-theoretical expression for $\mathbf{G}(\mathbf{x}',\mathbf{x}^s,\omega)$ into equation B-7. The ray-theoretical Green's function in homogeneous anisotropic media is given by (Červený, 2001)

$$\mathbf{G}(\mathbf{x}',\mathbf{x}^s,\omega) = g_i(\mathbf{x}')g_k(\mathbf{x}')\frac{1}{4\pi c(\mathbf{x}^s)\sqrt{\det[\mathbf{Q}_2(\mathbf{x}',\mathbf{x}^s)]}} \times\exp(-i\omega\tilde{T}(\mathbf{x}',\mathbf{x}^s)). \tag{B-8}$$

Combining equations B-7 and B-8 allows us to obtain the weighting function:

$$\Phi(\theta_0) = \sqrt{\frac{\omega}{2\pi}}\sqrt{\frac{\det[\tilde{\mathbf{W}}(\mathbf{x}',\mathbf{x}^s)]}{\det[\mathbf{Q}_2(\mathbf{x}',\mathbf{x}^s)]}\left.\frac{\partial^2\psi}{\partial\gamma^2}\right|_{\gamma=0}}. \tag{B-9}$$

REFERENCES

Alkhalifah, T., 1995, Gaussian beam depth migration for anisotropic media: Geophysics, **60**, 1474–1484, doi: 10.1190/1.1443881.

Aminzadeh, F., N. Burkhard, J. Long, T. Kunz, and P. Duclos, 1996, Three dimensional SEG/EAGE models — An update: The Leading Edge, **15**, 131–134, doi: 10.1190/1.1437283.

Behura, J., and I. Tsvankin, 2009a, Estimation of interval anisotropic attenuation from reflection data: Geophysics, **74**, no. 6, A69–A74, doi: 10.1190/1.3191733.

Behura, J., and I. Tsvankin, 2009b, Reflection coefficients in attenuative anisotropic media: Geophysics, **74**, no. 5, WB193–WB202, doi: 10.1190/1.3142874.

Bleistein, N., 1984, Mathematical methods for wave phenomena: Academic Press.

Bleistein, N., 1986, Two-and-one-half dimensional in-plane wave propagation: Geophysical Prospecting, **34**, 686–703, doi: 10.1111/j.1365-2478.1986.tb00488.x.

Bleistein, N., 2008, Seismic wavefields in layered isotropic media (course notes): CWP, Colorado School of Mines, http://www.cwp.mines.edu/norm/ShrtCrse, accessed 1 May 2013.

Bulant, P., 1996, Amplitude and phase data inversion for phase velocity anomalies in the Pacific Ocean basin: Pure and Applied Geophysics, **148**, 421–447, doi: 10.1007/BF00874574.

Carcione, J., 1990, Wave propagation in anisotropic linear viscoelastic media: Theory and simulated wavefields: Geophysical Journal International, **101**, 739–750, doi: 10.1111/j.1365-246X.1990.tb05580.x.
Carcione, J., 2010, A generalization of the Fourier pseudospectral method: Geophysics, **75**, no. 6, A53–A56, doi: 10.1190/1.3509472.
Červený, V., 1985, Gaussian beam synthetic seismograms: Journal of Geophysics, **58**, 44–72.
Červený, V., 2001, Seismic ray theory: Cambridge University Press.
Červený, V., and I. Pšenčik, 2009, Perturbation Hamiltonians in heterogeneous anisotropic weakly dissipative media: Geophysical Journal International, **178**, 939–949, doi: 10.1111/j.1365-246X.2009.04218.x.
Červený, V., and I. Pšenčik, 2010, Gaussian beams in inhomogeneous anisotropic layered structures: Geophysical Journal International, **180**, 798–812, doi: 10.1111/j.1365-246X.2009.04442.x.
Chapman, C., 2004, Fundamentals of seismic wave propagation: Cambridge University Press.
Futterman, W. I., 1962, Dispersive body waves: Journal of Geophysical Research, **67**, 5279–5291, doi: 10.1029/JZ067i013p05279.
Gajewski, D., and I. Pšenčik, 1992, Vector wavefield for weakly attenuating anisotropic media by the ray method: Geophysics, **57**, 27–38, doi: 10.1190/1.1443186.
Hale, D., 1992, Computational aspects of Gaussian beam migration: CWP Research Report 121.
Hanyga, A., and M. Seredyňska, 2000, Ray tracing in elastic and viscoelastic media: Pure and Applied Geophysics, **157**, 679–717, doi: 10.1007/PL00001114.
Hill, R. N., 1990, Gaussian beam migration: Geophysics, **55**, 1416–1428, doi: 10.1190/1.1442788.
Jakobsen, M., and M. Chapman, 2009, A unified theory of global flow and squirt flow in cracked porous media: Geophysics, **74**, no. 2, WA65–WA76, doi: 10.1190/1.3078404.
Johnston, D. H., and M. Toksöz, 1981, Seismic wave attenuation: SEG.
Kjartannson, E., 1979, Constant *Q*-wave propagation and attenuation: Journal of Geophysical Research, **84**, 4737–4748, doi: 10.1029/JB084iB09p04737.
Liu, H.-P., D. L. Anderson, and H. Kanamori, 1976, Velocity dispersion due to anelasticity; implications for seismology and mantle composition: Geophysical Journal of the Royal Astronomical Society, **47**, 41–58, doi: 10.1111/j.1365-246X.1976.tb01261.x.
Liu, J., and G. Palacharla, 2010, Kirchhoff beam *Q* migration: 72nd Annual International Conference and Exhibition, EAGE, Extended Abstracts, C015.
Mallick, S., and N. L. Frazer, 1990, Computation of synthetic seismograms for stratified azimuthally anisotropic media: Journal of Geophysical Research, **95**, 8513–8526, doi: 10.1029/JB095iB06p08513.
Rüger, A., 1997, P-wave reflection coefficients for transversely isotropic models with vertical and horizontal axis of symmetry: Geophysics, **62**, 713–722, doi: 10.1190/1.1444181.
Ruud, B. O., and S. Hestholm, 2005, Modeling seismic waves in orthorhombic, viscoelastic media by finite-differences: 75th Annual International Meeting, SEG, Expanded Abstracts, 1771–1774.
Schmidt, H., and G. Tango, 1986, Efficient global matrix approach to the computation of synthetic seismograms: Geophysical Journal of the Royal Astronomical Society, **84**, 331–359, doi: 10.1111/j.1365-246X.1986.tb04359.x.
Shekar, B., and I. Tsvankin, 2012, Attenuation analysis for heterogeneous transversely isotropic media: 82nd Annual International Meeting, SEG, Expanded Abstracts, doi: 10.1190/segam2012-1489.1.
Stockwell, J. W., 1999, The CWP/SU: Seismic Un*x Package: Computers & Geosciences, **25**, 415–419, doi: 10.1016/S0098-3004(98)00145-9.
Thomson, C. J., 1997, Complex rays and wave packets for decaying signals in inhomogeneous, anisotropic and anelastic media: Studia Geophysica et Geodaetica, **41**, 345–381, doi: 10.1023/A:1023359401107.
Tsvankin, I., and V. Grechka, 2011, Seismology of azimuthally anisotropic media and seismic fracture characterization: SEG.
Xu, T., and G. A. McMechan, 1998, Efficient 3-D viscoelastic modeling with application to near-surface land seismic data: Geophysics, **63**, 601–612, doi: 10.1190/1.1444359.
Yomogida, K., and K. Aki, 1987, Amplitude and phase data inversion for phase velocity anomalies in the Pacific Ocean basin: Geophysical Journal of the Royal Astronomical Society, **88**, 161–204, doi: 10.1111/j.1365-246X.1987.tb01374.x.
Zhang, Y., P. Zhang, and H. Zhang, 2010, Compensating for visco-acoustic effects with reverse time migration: 80th Annual International Meeting, SEG, Expanded Abstracts, 3160–3164.
Zhu, Y., and I. Tsvankin, 2006, Plane-wave propagation in attenuative transversely isotropic media: Geophysics, **71**, no. 2, T17–T30, doi: 10.1190/1.2187792.
Zhu, Y., I. Tsvankin, P. Dewangan, and K. V. Wijk, 2007, Physical modeling and analysis of P-wave attenuation anisotropy in transversely isotropic media: Geophysics, **72**, no. 1, D1–D7, doi: 10.1190/1.2374797.